Ceramics-Silikáty 66 (3), 310-324 (2022)
www.ceramics-silikaty.cz doi: 10.13168/cs.2022.0027

INFLUENCE OF THE CaO CONTENT IN GLASS ON THE SINTERABILITY AND PROPERTIES OF A GLASS/Al_2O_3 COMPOSITE FOR LTCC APPLICATIONS

YUNFEI FAN, #FENG HE, ZIJIE LI, JUNLIN XIE

School of Materials Science and Engineering, Wuhan University of Technology, Wuhan 430070, China

#E-mail: he-feng2002@163.com

Submitted April 15, 2022; accepted May 27, 2022

Keywords: Low-temperature co-fired ceramic, $CaO–B_2O_3–Al_2O_3–SiO_2$ glass, sinterability, flexural strength

In this paper, the influence of the CaO content in glass on the sintering behaviour, structure, and properties of $CaO–B_2O_3–Al_2O_3–SiO_2$ glass/Al_2O_3 composites for low-temperature co-fired ceramic materials was studied. The results show that an increase in the CaO content in the glass reduces the polymerisation degree of the glass network, thereby reducing the glass viscosity and promoting the densification of the liquid phase sintering, increasing the crystallisation tendency of the material, reducing the crystallisation peak temperature and promoting the precipitation of anorthite in the material. The sintering activation energy of the glass/Al_2O_3 first decreases and then increases, and reached a minimum in C4. The anorthite can reduce the bulk density and coefficient of the thermal expansion of the materials, and an appropriate amount of anorthite can improve the flexural strength of the material by more than 190 MPa. When the CaO content in the glass increases, the required sintering temperature for the material to achieve the maximum flexural strength is lower. The sample (C4-850) with a CaO content of 27.60 %, achieving densification when sintered at 850 °C for 1 h, showed a flexural strength of 190.1 MPa and a coefficient of thermal expansion of 6.083 × 10^{-6} K^{-1}, which is suitable for substrate packaging.

INTRODUCTION

With the development of modern information technology, electronic and microelectronic devices are moving in the direction of being miniaturised, highly integrated, and highly efficient, with a high transmission speed [1, 2], which proposes new challenges to packaging materials and technologies for integrated substrates. The low-temperature co-fired ceramic (LTCC) technology is a multilayer substrate process technology that can be used to manufacture three-dimensional ceramic modules embedded with highly conductive metal electrodes and passive components [3, 4]. At the same time, LTCC materials have a lower sintering temperature, coefficient of thermal expansion (CTE) which when adapted to semiconductor materials of high thermal conductivity, are suitable for electronic substrate packaging [5, 6]. In order to realise the miniaturisation of electronic substrates, LTCC materials are required to have excellent mechanical properties to ensure mechanical reliability against assembly stress and drop impacts [7].

LTCC materials reduce the sintering temperature by introducing a glass phase, so that they can be co-fired with a low melting point and highly conductive metals [8]. LTCC materials include glass-ceramic systems and glass/ceramic systems [9-11], the latter were widely studied by adjusting the glass components and ceramic types to obtain LTCC systems with different properties. The glass/ceramic systems are formed through liquid phase sintering, which is completed by the glass liquid bonding the ceramic particles at a high temperature and the precipitation of crystalline phases [12]. The densification, crystalline phases, and ceramic types all have an impact on the performance of LTCC materials. Some of the main typical ceramic fillers include: Al_2O_3 [13, 14], AlN [15], Mg_2SiO_4 [16], β-spodumene [17] and so on. Among them, Al_2O_3 has a large Young's modulus, which can improve the flexural strength of LTCC materials as a ceramic matrix [18].

At present, research on LTCC materials of glass/ceramic systems has mostly focused on the glass/ceramics ratio and the sintering temperature, and there is little research on glass compositions. Changes in the glass compositions can adjust the wettability of the glass to the ceramic and the fluidity of the glass liquid under high temperatures, thereby improving the material densification [19, 20]. Luo et al. [21] studied the influence of the Al_2O_3 content change on the CABS glass/Al_2O_3 sintering in a glass. The increase in the Al_2O_3 content improved the wettability of the CABS glass to the Al_2O_3 filler, when the content was 4 wt. %, the flexural strength reached 206 MPa. Wang et al. [22] studied the effect of B_2O_3/SiO_2 in glass on the sintering behaviour of $La_2O_3–CaO–B_2O_3–SiO_2$ glass/Al_2O_3. The increase in SiO_2 content had little effect on the glass network structure, but it improved the densification degree and flexural strength of the LTCC materials.

As an alkaline earth metal oxide, CaO can change the degree of polymerisation of the glass network and affect the sintering behaviour, which has been studied in glass-ceramic systems many times. Yan et al. [23] studied the influence of CaO/SiO_2 on the sintering behaviour of $CaO–B_2O_3–SiO_2$ glass-ceramics and found that the increase in the CaO/SiO_2 ratio would reduce the degree of glass network polymerisation, increase the sintering shrinkage and decrease the crystallisation temperature. Shang et al. [24] added a small amount of CaO to a $K_2O–B_2O_3–SiO_2–Al_2O_3$ glass to improve the material densification and obtained a glass-ceramic with flexural strength of 173 MPa. For glass/ceramic system of LTCC materials, studies have shown that a $CaO\text{-}B_2O_3\text{-}SiO_2/Mg_2Al_4Si_5O_{18}$ [25], $CaO–Al_2O_3–B_2O_3–SiO_2/Al_2O_3$ [26] system glass sintering will react to form a strong phase interface, which is conducive to the wettability of the glass to the ceramic filler and improves the densification of the materials, and the formed anorthite phase can also improve the flexural strength. The CaO content of the glass in these studies was generally high (> 35 wt. %).

At present, the CaO content in the parent glass of the $CaO–B_2O_3–Al_2O_3–SiO_2$ glass/Al_2O_3 composite system is generally lower than 20 wt. %. Therefore, this study increases the CaO content in the glass to within the range of 20 ~ 30 wt. %, investigates the influence of the change of the CaO content in the glass on the sinterability, structure and properties of the LTCC materials, and obtains a low cost LTCC material having a low sintering temperature and a high flexural strength.

EXPERIMENTAL

The composition of the $CaO–B_2O_3–Al_2O_3–SiO_2$ (CBAS) glass is shown in Table 1. Analytical grade $CaCO_3$, H_3BO_3, Al_2O_3, SiO_2, K_2CO_3, Li_2CO_3, and ZrO_2 were used as the raw materials in laboratory. The accurately weighed and fully mixed raw materials were melted at 1450 °C for 2 h with a heating rate of 5 °C·min^{-1}. The molten glass liquid was poured into a mould, and annealed at 550 °C for 1 h. The glass was crushed, ball milled and screened to obtain a glass powder with an average particle size of 4 ~ 5 μm. The CBAS parent glass powder, fused silica powder, and micron alumina ball were mixed uniformly according to the mass ratio of 45:5:50, and the obtained powder was granulated by adding a certain amount of a Polyvinyl Alcohol (PVA) solution (5 wt. %), and then kept under 30 kN pressure for 5 min to make a green body. The green body was heated to the specified temperature with a heating rate of 5 °C·min^{-1} in air and kept at the temperature for 1 h to obtain experimental samples.

Table 1. Composition of the CBAS glasses (wt. %).

	CaO	B_2O_3	Al_2O_3	SiO_2	K_2O	Li_2O	ZrO_2
C1-G	21.60	8.20	12.50	51.90	0.80	2.00	3.00
C2-G	23.60	8.20	12.50	49.90	0.80	2.00	3.00
C3-G	25.60	8.20	12.50	47.90	0.80	2.00	3.00
C4-G	27.60	8.20	12.50	45.90	0.80	2.00	3.00
C5-G	29.60	8.20	12.50	43.90	0.80	2.00	3.00

The structure of the parent glasses was tested and analysed by Fourier transform infrared spectrometer (FTIR, Nicolet 6700) and laser confocal Raman microscope (Raman, LABHRev-UV). A thermal analysis was performed on the parent glasses and glass/Al_2O_3 samples by differential scanning calorimetry (DSC; STA449F3) from the ambient temperature to 1000 °C in air at a heating rate of 5 °C·min^{-1}. The sintering shrinkage curve of the parent glasses and glass/Al_2O_3 was measured by a heating microscope (HTM, HM867). The crystalline phase composition of the sintered samples was measured by X-ray diffractometer (XRD, D8 Advance), with a test range of 10 ~ 70°. A cross-section of the sintered samples was taken using a field emission scanning electron microscope with an X-Max 50 X-ray energy spectrometer (SEM, ULTRA PLUS) in order to photograph the microstructure and scan the energy spectrum, and some samples were acid-etched before testing. The bulk density of the sintered samples was measured by the Archimedes drainage method using a Shimadzu balance. The flexural strength of the sintered samples was measured by three-point bending method using a KZY-300-1 universal testing machine. The CTE of the sample was determined using a thermal dilatometer (CTE, DIL 402c).

RESULTS AND DISCUSSION

Structural analysis of the parent glasses

Figure 1 shows the FTIR spectra of the parent glasses with different CaO content, with the corresponding vibrations listed in Table 2. It can be seen from Figure 1 that the FTIR spectra of CBAS glasses substantially have the same shape, including four absorption peak bands near 475 cm^{-1}, 715 cm^{-1}, 1020 cm^{-1} and 1415 cm^{-1}.

According to the literatures, the vibration peak near 475 cm^{-1} is attributed to the bending vibration of Si–O–Si in [SiO_4] and Si–O–Al between [SiO_4] and [AlO_4] [27], the vibration peak near 715 cm^{-1} is attributed to the bending vibration of B–O–B in [BO_3] and the symmetrical stretching vibration of Si–O–Al between [SiO_4] and [AlO_4] [28]. With an increase in the CaO content in the glass, the free oxygen introduced by CaO promotes the transformation of [AlO_6] into [AlO_4], thereby the Si–O–Al bond connecting [SiO_4] and [AlO_4] gradually increases, resulting in both of them moving from a low wave number segment to a high wave number segment, and the peak intensity of the vibration peak near 715 cm^{-1} is gradually enhanced. The free oxygen not only satisfies the transformation of [AlO_6] into [AlO_4] in the glasses, but also promotes the transformation of

[BO_3] into [BO_4] in the glasses. The vibration peak near 1415 cm^{-1} is attributed to the stretching vibration of the B–O–B in [BO_3] [29], its absorption band shifts from a high wave number band to a low wave number band which confirms the reduction of [BO_3] in the glasses.

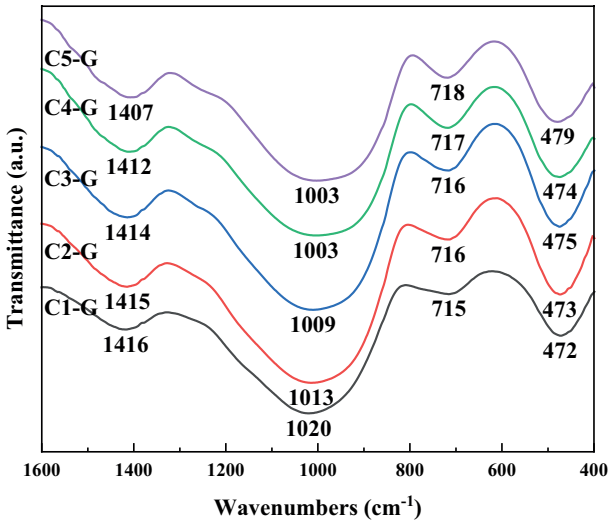

Figure 1. FTIR spectra of the parent glasses with the different CaO content.

Table 2. The vibrating groups of the FTIR spectra of the parent glasses.

Wave number (cm^{-1})	Corresponding characteristic vibration
475	Bending vibration of Si–O–Si and Si–O–Al
715	Bending vibration of B–O–B and symmetrical stretching vibration of Si–O–Al
1020	Asymmetric stretching vibration of Si–O–Si
1415	Stretching vibration of B–O–B

The absorption band near 1020 cm^{-1} is the stretching vibration of the bridging oxygen, which is mainly attributed to the asymmetric stretching vibration of Si–O–Si in [SiO_4] [30]. With an increase in the CaO content in the glass, the absorption peak bands near 1020 cm^{-1} moved from a high wave number segment to a low wave number segment and the peak intensity gradually weakened. The literature shows that when the degree of polymerisation in the glass network structure decreases, the corresponding infrared vibration band will move to a lower wave number [31]. As an alkaline earth metal oxide, CaO acts as a glass network modifier in the glass structure. Ca^{2+} has a larger field strength than Si^{4+}, causing the rupture of the Si–O–Si in [SiO_4], resulting in depolymerisation of the siloxane anion cluster in the silicate network structure into a simpler structural unit [32]. Therefore, the absorption peak near 1020 cm^{-1} produces such a change. At the same time, because [AlO_6] and [BO_3] in the glasses are transformed into [AlO_4] and [BO_4] in the glass network structure, but is limited by the principle of tetrahedral repulsion, [BO_4] and [BO_4], [BO_4] and [AlO_4], [AlO_4] and [AlO_4] cannot be connected to each other, and can only be connected by the electrically neutral [SiO_4].Therefore, the main bridging oxygen types in the absorption band near 1020 cm^{-1} and the left and right shoulders are Si–O–Si, B–O––Si, Si–O–Al. With an increase in the CaO content in the glass, the left shoulder of the absorption band near 1020 cm^{-1} is gradually enhanced, which means that the B–O–Si between [BO_4] and [SiO_4] gradually increases, indicating that the [BO_4] content in the glass network structure gradually increases, which is consistent with the shift in the absorption band near 1415 cm^{-1} from a high wave number segment to a low wave number segment. In summary, although the increase in CaO content promotes the transformation of [AlO_6] and [BO_3] into [AlO_4] and [BO_4] in the glass network to promote the glass network polymerisation degree, it is difficult to compensate for the reduction of [SiO_4] in the network structure, therefore, the polymerisation degree of the glass network decreases as a whole.

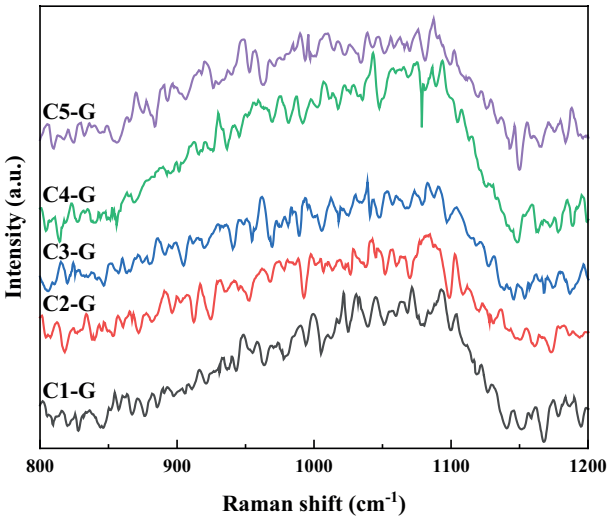

Figure 2. Raman spectra of the CBAS glasses with the different CaO content.

Figure 2 shows the Raman spectra of parent glasses with the different CaO contents. It can be seen that each group of parent glass has an obvious broad ranging band in the Raman shift range of 800 ~ 1200 cm^{-1}, which is attributed to the stretching vibration of Si–O in [SiO_4] with the different bridge oxygen contents [33]. The broad ranging band was deconvoluted based on Gaussian function for the determination of the proportions of Q^n (n is the bridging oxygen number, n = 0, 1, 2, 3, 4) in the parent glasses, which were represented by the area fraction of the fitting peak. According to the literatures [34], Q^0 is located near 880 cm^{-1}, Q^1 is located near 930 cm^{-1}, Q^2 is located near 990 cm^{-1}, Q^3 is located near

1050 cm^{-1} and Q^4 is located near 1150 cm^{-1}. Figure 3 shows the deconvolution of the Raman spectra of the parent glasses with the different CaO contents, and the area fraction of the Q^n obtained from the Gaussian deconvolution of the Raman spectra listed in Table 3. The coefficient of determination R^2 > 99 % showed that the deconvolved results are effective and reliable. There are three fitting peaks in a broad ranging band, which are located near 920 cm^{-1}, 990 cm^{-1} and 1070 cm^{-1}, corresponding to Q^1, Q^2 and Q^3, respectively.

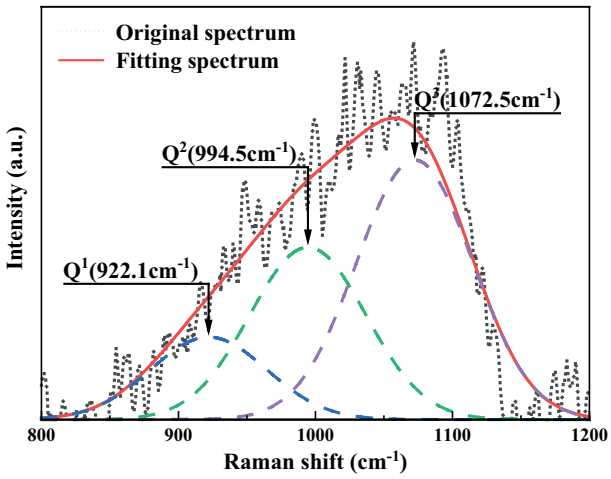

a) C1-G

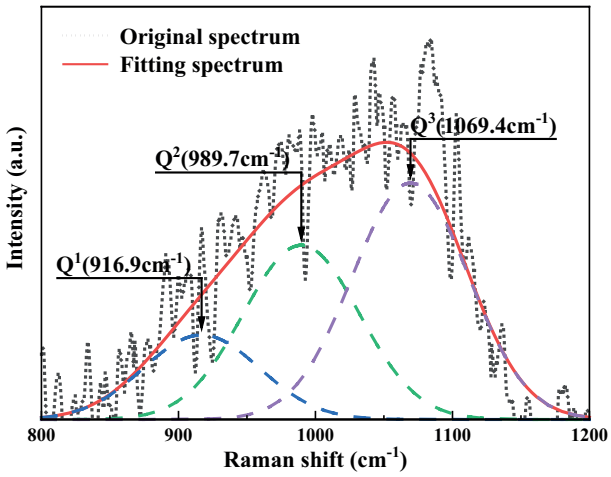

b) C2-G

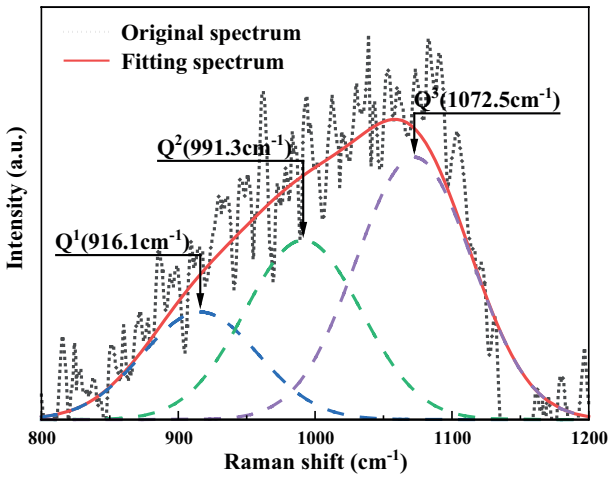

c) C3-G

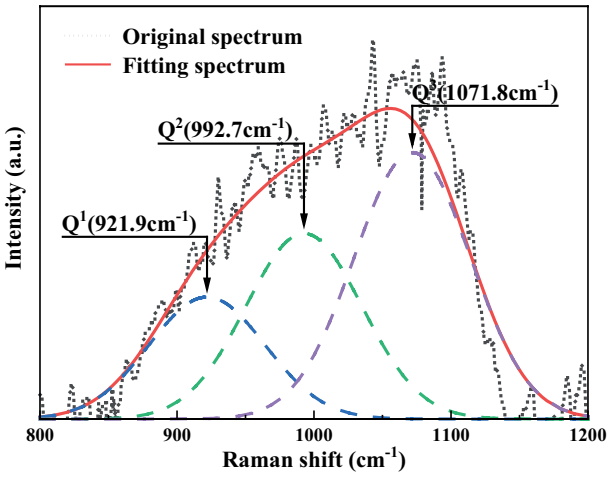

d) C4-G

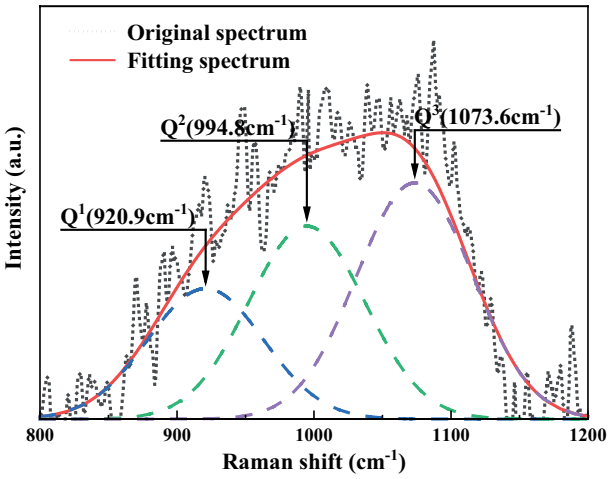

e) C5-G

Figure 3. Deconvolved Raman spectra of the parent glasses.

Table 3. Area fraction of Q^n (%).

	Q^1	Q^2	Q^3	R^2
C1-G	15.98	33.76	50.26	99.85
C2-G	16.95	35.54	47.51	99.69
C3-G	19.44	32.95	47.61	99.81
C4-G	21.12	32.57	46.31	99.83
C5-G	23.15	34.77	42.09	99.82

Figure 4 shows the change curves of the area fraction of Q^n. With an increase in the CaO content in the glass, the relative content of Q^1 gradually increases, the relative content of Q^2 does not change much, and the relative content of Q^3 gradually decreases, which means that the

increase in the CaO content in the glass promotes the transformation of Q^3 into Q^1, the polymerisation degree of the glass network has decreased, which is consistent with the FTIR analysis results.

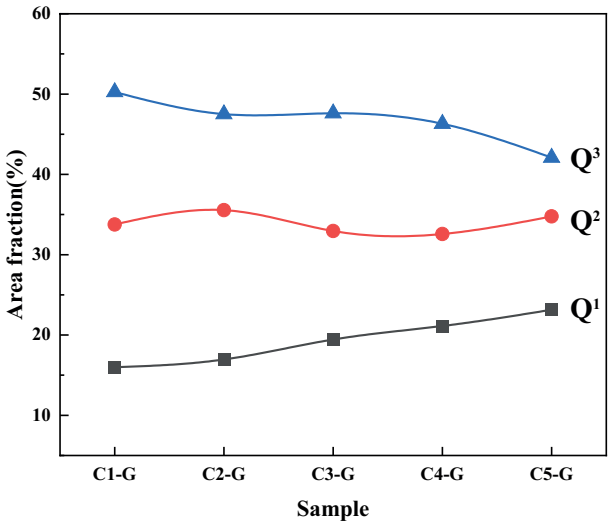

Figure 4. The change curves of the area fraction of Q^n.

Thermal analysis of parent glasses

Figure 5 shows the DSC curves of the parent glasses with the different CaO content, the characteristic temperature of the DSC curves from ambient temperature to 1000 ℃ listed in Table 4, where T_g is the glass transition temperature, T_s is the sintering temperature, and T_p is the crystallisation peak temperature.

It can be seen from Figure 5 that each curve has an inflection point near 620 ℃, here it is denoted as T_g. When the temperature reaches 720 ℃, each curve begins to decrease, where the endothermic peak reflects

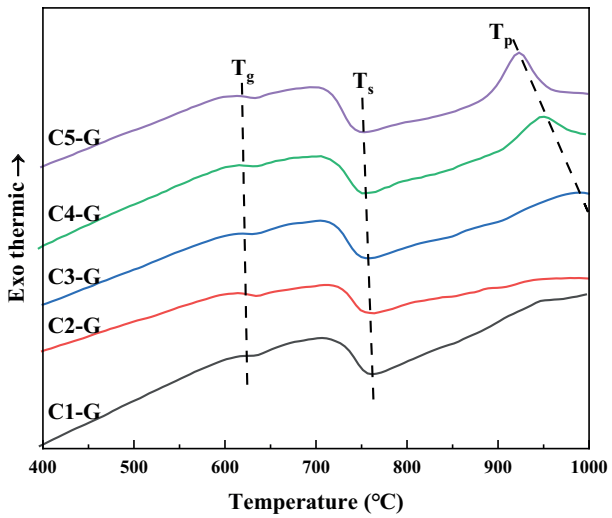

Figure 5. DSC curves of the parent glasses with the different CaO content.

the sintering of the glass powder, T_s is around 755 ℃. Then each curve gradually rises, and the crystallisation peak starts to appear from C3-G, and T_p is in the range of 920 ~ 1000 ℃. It can be seen from Table 4 that as the CaO content increases (C1-G→C5-G), the T_g and T_s of the glasses show a gradual decreasing trend. With an increase in the CaO content in the glass, the polymerisation degree of the glass network decreased, which caused the glass transition temperature to decrease. Glass powder sintering belongs to liquid phase sintering, where the viscosity of the glass is reduced, and the T_s required for the sintering densification under the action of capillary force is reduced [35]. With an increase in the CaO content in the glass, the T_p gradually decreases, and the peak gradually increases. It is reasonable to believe that the increase in the CaO content is beneficial to the precipitation of crystals.

Table 4. DSC characteristic temperatures of the parent glasses (℃).

Number	T_g	T_s	T_p
C1-G	624	762	—
C2-G	623	762	—
C3-G	621	757	990
C4-G	620	754	949
C5-G	619	752	923

HTM was used to perform the sintering test on the glass powder to obtain the sintering shrinkage diagrams of the parent glasses with the different CaO content as shown in Figure 6. The increase in the CaO content in the glass led to a decrease in the softening temperature and sphere temperature of the glasses, and an increase in the hemisphere temperature and melting temperature. The softening temperature and spheroidizing temperature of the glasses reflect the fluidity of the glass liquid. The gradual decrease in their values means that the fluidity of the glass liquid is enhanced at the same temperature, which is beneficial to the liquid phase sintering. As the temperature continued to rise, the crystalline phase

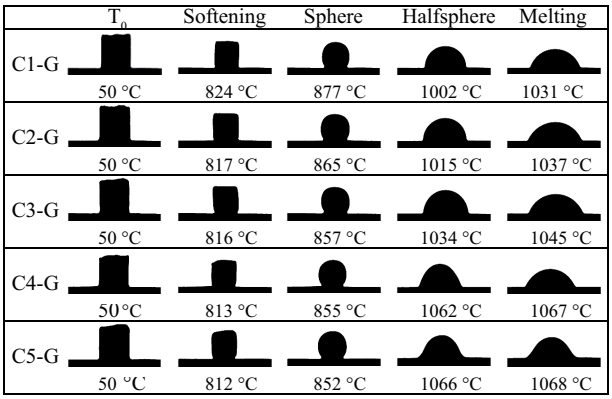

Figure 6. Sintering shrinkage diagrams of the parent glasses with the different CaO content.

appeared in the sample, which kept the shape of the sample fixed, thereby leading to an increase in the hemisphere temperature and melting temperature of the test result.

Thermal analysis of CBAS glass/Al_2O_3

Figure 7 shows the DSC curves of the CBAS glass mixtures with the different CaO, fused silica powder, and micron alumina ball content, where T_{p*} is the crystallisation peak temperature. With the increase in the CaO content in the glass, the T_{p*} gradually decreases, and the peak intensity gradually increases. The DSC curves of the glass/Al_2O_3 were greatly different from the parent glasses, which means that as the temperature increases, not only the liquid phase sintering process and crystalline phase precipitation of the glass occur inside the sample, but also the diffusion and phase reaction of Al_2O_3 in the glass. Studies have shown that Al_2O_3 will partially dissolve in glass at high temperatures, changing the composition of the glass, and promote the precipitation of crystal phases [36].

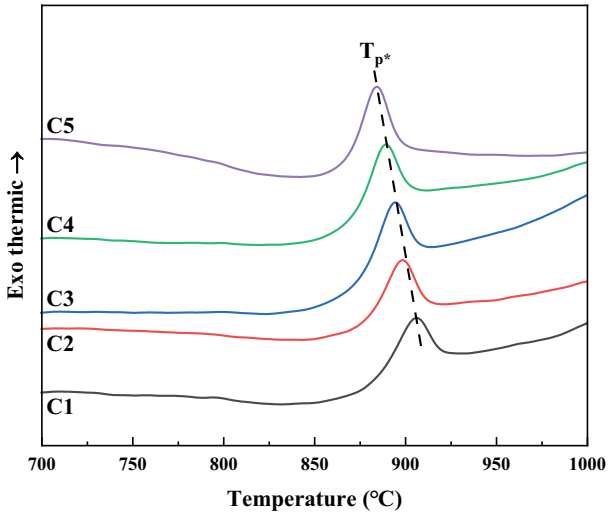

Figure 7. DSC curves of the CBAS glass/Al_2O_3.

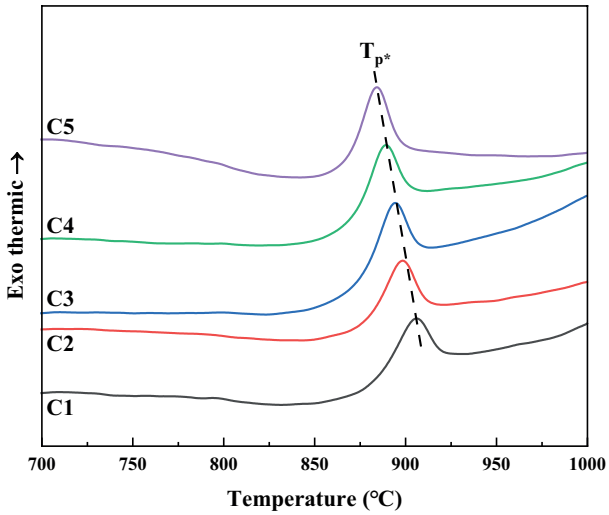

Figure 8. Sintering shrinkage curve and DSC curve of the C3 group glass/Al_2O_3.

Figure 8 shows the sintering shrinkage curve and the DSC curve of the C3 group glass/Al_2O_3. As the temperature increased, the sample slightly expanded to the starting temperature of the liquid phase sintering T_{FS}, and then began to shrink sharply. At the densification point temperature T_{MS}, the sample volume reached a minimum, and then the sample volume gradually expanded. Table 5 lists some characteristic temperatures of the CBAS glass/Al_2O_3. It can be seen that as the CaO content in the glass increases, the T_{FS} of the sample does not change much, indicating that it has little effect on the initial stage of sintering. The T_{MS} gradually decreases with the increase in the CaO content. Due to the decreases in the degree of polymerisation of the glass network, the glass fluidity increases at the same temperature, so that the sintering densification process is completed early, resulting in a T_{MS} decrease. The sinterability parameter, denoted as ΔT, can be calculated by the formula:

$$\Delta T = T_{p*} - T_{MS} \quad (1)$$

reflecting the independence of the crystallisation and sintering process, the larger the ΔT, the more independent the two variables are. Studies have shown that the crystallisation can inhibit the flow of the liquid phase and affect the sintering progress. With an increase in the CaO content in the glass, ΔT first increased and then decreased, reaching the maximum at C3, indicating that the C3 sample is easier to achieve densification during the sintering process.

Table 5. Characteristic temperatures of the CBAS glass/Al_2O_3.

Number	T_{FS} (°C)	T_{MS} (°C)	T_p* (°C)	ΔT (°C)^2
C1	726	884	906	22
C2	727	852	898	46
C3	725	843	894	51
C4	722	839	889	50
C5	726	837	884	47

In order to better study the sintering behaviour, this experiment measured the sintering shrinkage curve at different heating rates to calculate the sintering activation energy. Figure 9 shows the sintering shrinkage curve of the CBAS glass/Al_2O_3 at 5 °C·min^{-1}, 10 °C·min^{-1}, 15 °C·min^{-1}, and 20 °C·min^{-1}. The sintering activation energy is calculated by Arrhenius' formula [37, 38]:

$$\ln k = -\frac{E_a}{RT} + A \quad (2)$$

where k is the heating rate, E_a is the sintering activation energy, T is the absolute temperature, R is the gas constant (8.3145 J·(K·mol^{-1})$^{-1}$), and A is a constant value. The fitting curves of 1000lnk and 1000/T were made

at the volume shrinkage rates of 5 %, 10 %, 15 % and 25 %, and the results are shown in Figure 10a-e. Figure 10f shows that with the increase in the CaO content in the glass, E_a shows a trend of first decreasing and then increasing, indicating that the C2~C4 samples are easier to sinter than C1 and C5.

Generally speaking, the sintering temperature should be set between T_{FS} and T_{p*}. Based on the test results of the DSC and HTM, the sintering temperatures selected in this experiment are 825 °C, 850 °C, 875 °C, 900 °C and 925 °C.

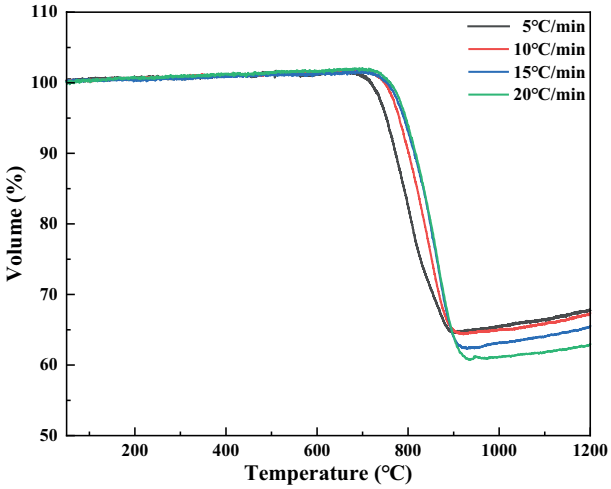

a) C1

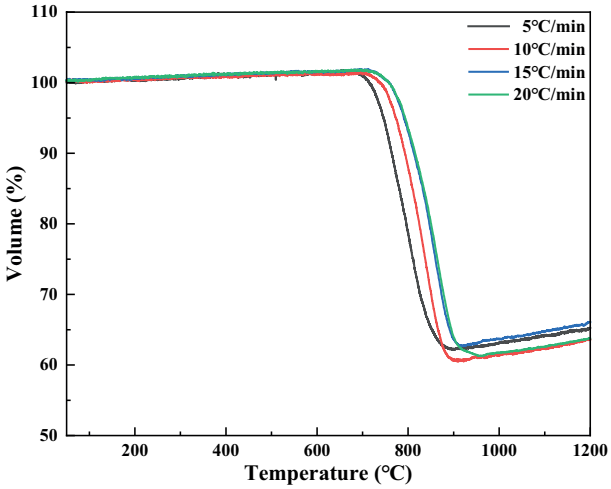

b) C2

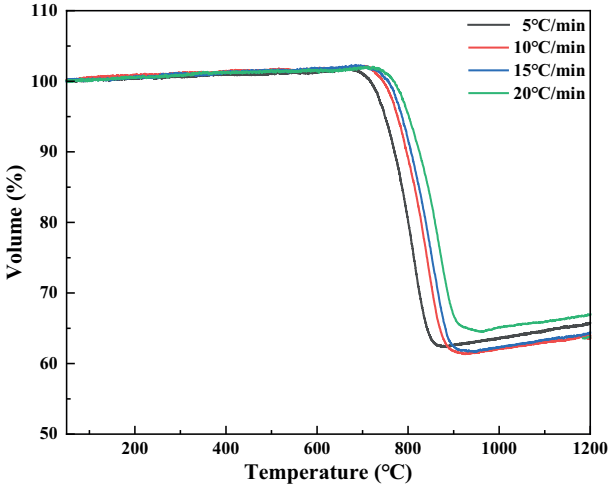

c) C3

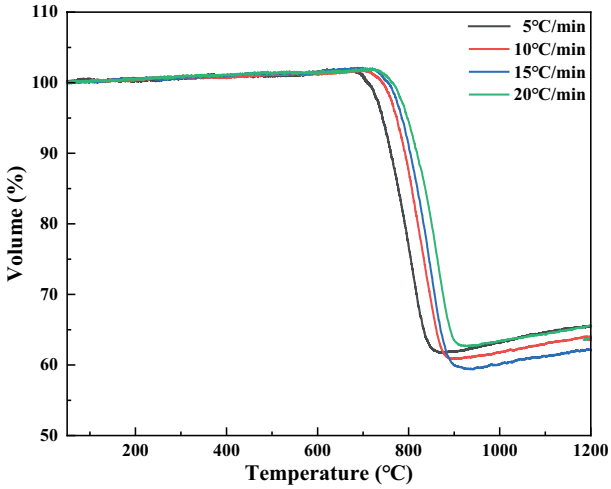

d) C4

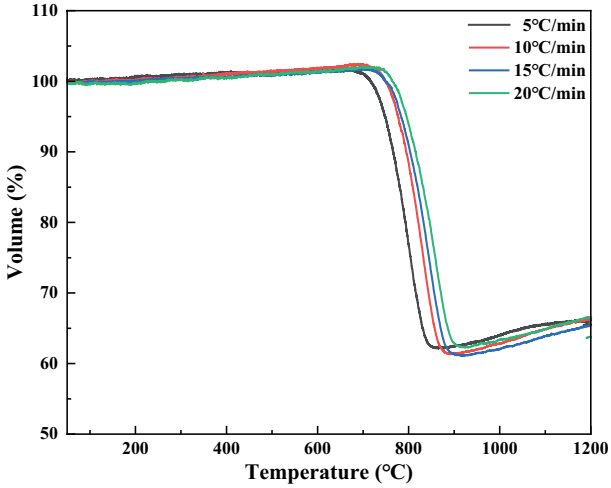

e) C5

Figure 9. Sintering shrinkage curve of the CBAS glass/Al_2O_3 at the different heating rates.

Structural analysis of sintered samples

Figure 11a shows the XRD curve of the micron alumina ball, which is composed of three crystal forms (Al_2O_3 PDF#78-2427, Al_2O_3 PDF#86-1410, Al_2O_3 PDF #46-1215). Figure 11a-e shows the XRD curves of the samples sintered at different temperatures. In addition to the introduced alumina, the crystalline phases in the samples also includes anorthite ($CaAl_2Si_2O_8$ PDF#41-1486), β-quartz solid solution ($Li_xAl_xSi_{1-x}O_2$ PDF#40-0073). Figure 11a shows the XRD curves of the samples sintered at 825 °C. C1-825 and C2-825 only have an alumina and β-quartz solid solution. With the

increase in the CaO content in the glass, the diffraction peak intensity of the β-quartz solid solution gradually decreased, and the anorthite diffraction peak intensity gradually increased, indicating that the content of them in the sample also changed accordingly. When the sintering temperature is 850 °C and above, the β-quartz solid solution diffraction peak is extremely weak, and there is only an obvious peak at 25.77°. As the CaO

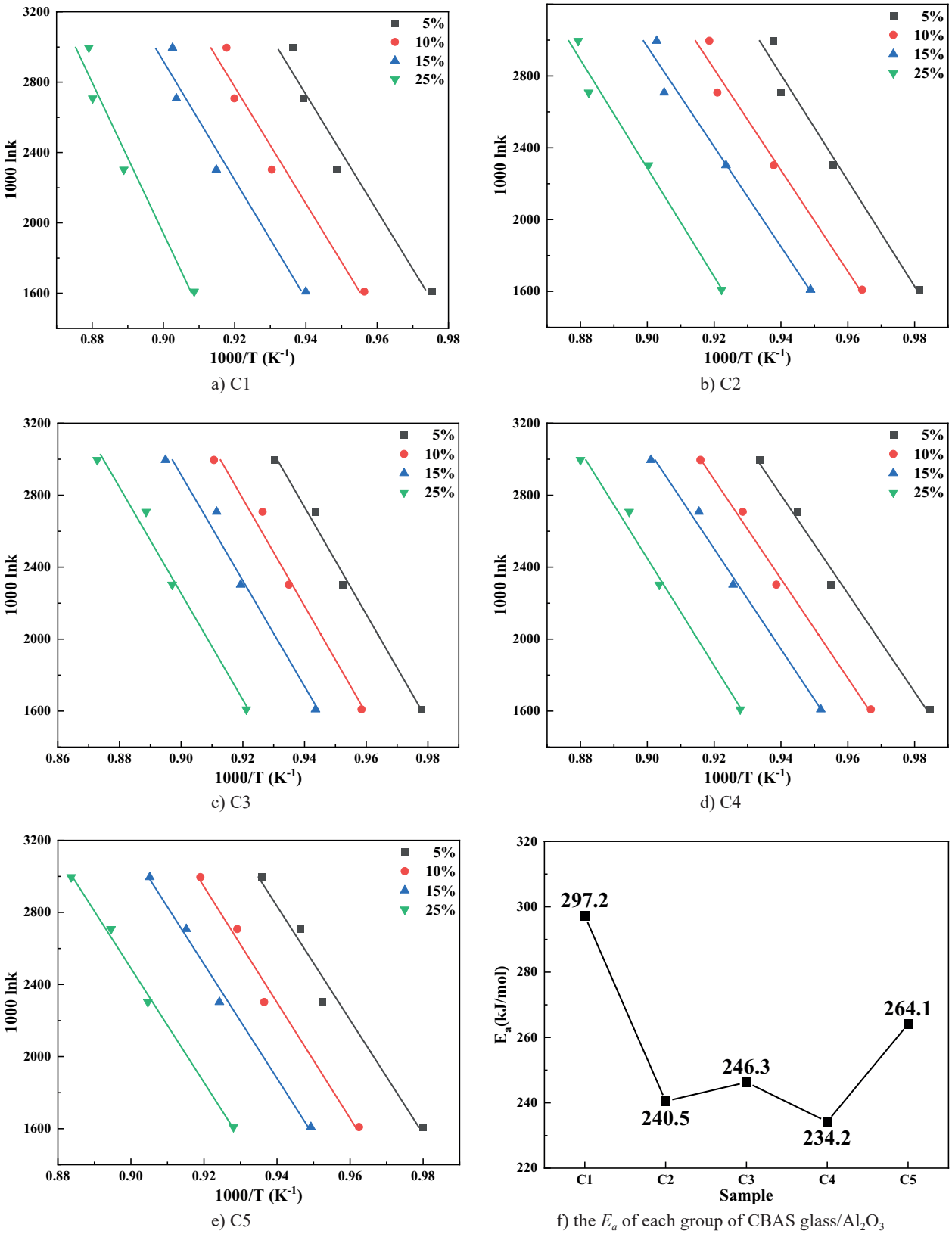

Figure 10. The relationship between 1000 ln *k* and 1000/*T* under the different shrinkage rates.

content in the glass increases, the content of alumina in the sample gradually decreases and the content of anorthite gradually increases, which means that CaO is beneficial to the precipitation of anorthite. For samples of the same composition, as the sintering temperature increases, the content of the β-quartz solid solution and alumina in the sample decreases, and the content of anorthite gradually increases. This is consistent with the results of the DSC curve. Increasing the temperature is beneficial to the precipitation of anorthite, especially the sintering temperature from 825 ℃ to 850 ℃.

Figure 12a shows the SEM morphology of the micron alumina balls, and their surface are relatively smooth before sintering. Figure 12b-d show the SEM morphologies of the cross-sections of samples C1, C3 and C5 sintered at 825 ℃. With ab increase in the CaO content in the glass, the number of pores in the sample gradually decreases and the size of the pores gradually increases. The section of the sample changes from smooth to rough, especially in the C5-825 image in which a striped texture can be clearly observed. This is because the increased CaO content in the glass led to a decrease in the degree of polymerisation of the glass network, which improved the fluidity of the glass liquid at the same temperature, which was conducive to filling the voids of the material under capillary force action by the glass liquid, so that the small pores converge into large pores [39]. In addition, The XRD results also indicate that there are more anorthite phases precipitated in the C5-825 sample. As a framework silicate mineral, anorthite has a triclinic crystal system, which is often plate-like or plate-columnar crystals, resulting in a rough section for the C5-825 sample. Figure 12c,e,f show the SEM morphologies of the cross-sections of the C3 samples sintered at 825 ℃, 875 ℃ and 925 ℃, respectively. Compared with C3-825, C3-875 and C3-925, they have rougher cross-sections and fewer pores. As the sintering temperature increases, the viscosity of the molten glass decreases, which is conducive to the glass liquid filling the pores. At the same time, the precipitation and coarsening of the anorthite inhibit the flow of the glass liquid phase and the gap increases, the cross-section became rough, and the pores even change from round to irregular in shape.

Figure 12g-i show the SEM morphologies of C3-825, C3-875 and C3-925 respectively, after being treated with a Hydrofluoric acid (HF) solution (4 vol. %) for 45 s. It can be clearly observed that the sample consists of homogeneously dispersed spheres, a columnar structure and a residual glassy phase. As the sintering temperature increases, the surface of the ball became rough, and the columnar structure gradually increased. The EDS Energy-dispersive X-ray spectroscopy) spectrum on the two points A and B is seen in Figure 12i and the result

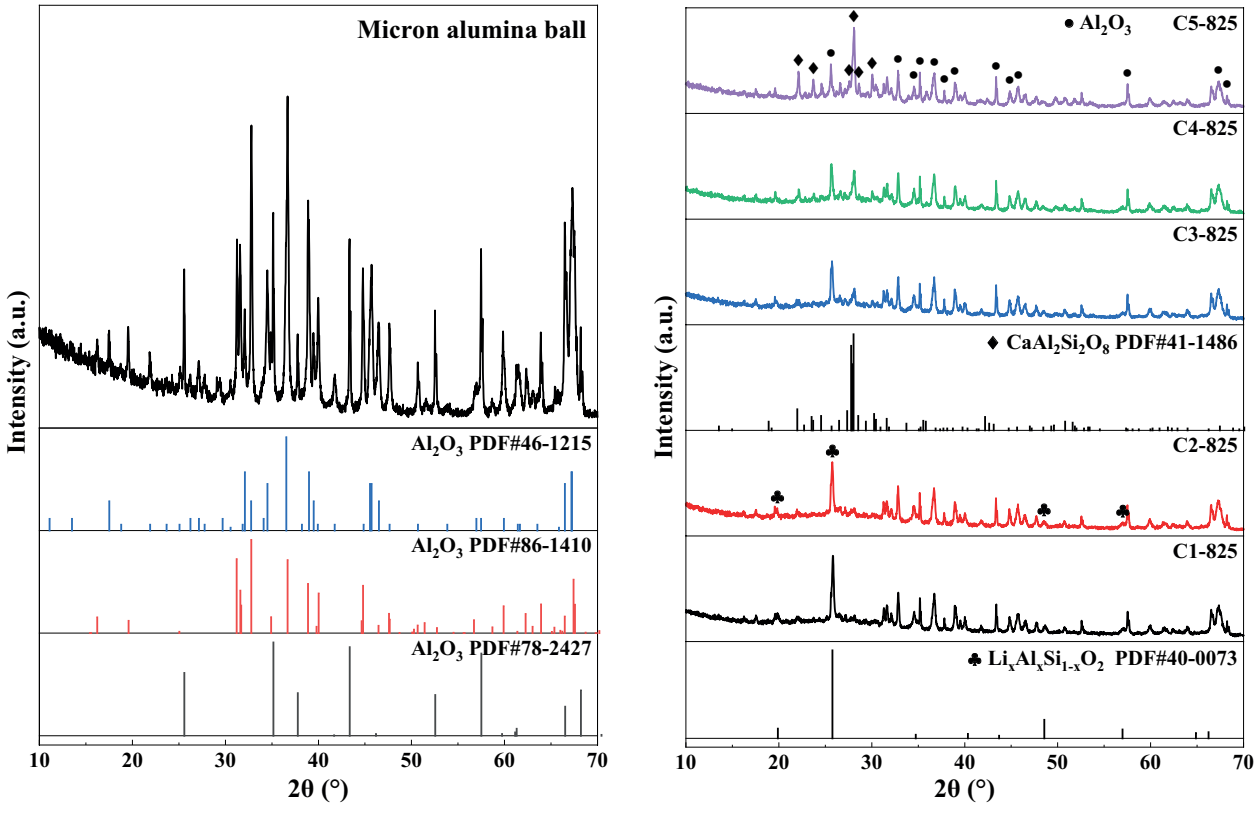

Figure 11. XRD curve of the micron alumina ball (a); XRD curves of the samples sintered at the different temperatures; b)-e): 825-925 ℃. *(Continue on next page)*

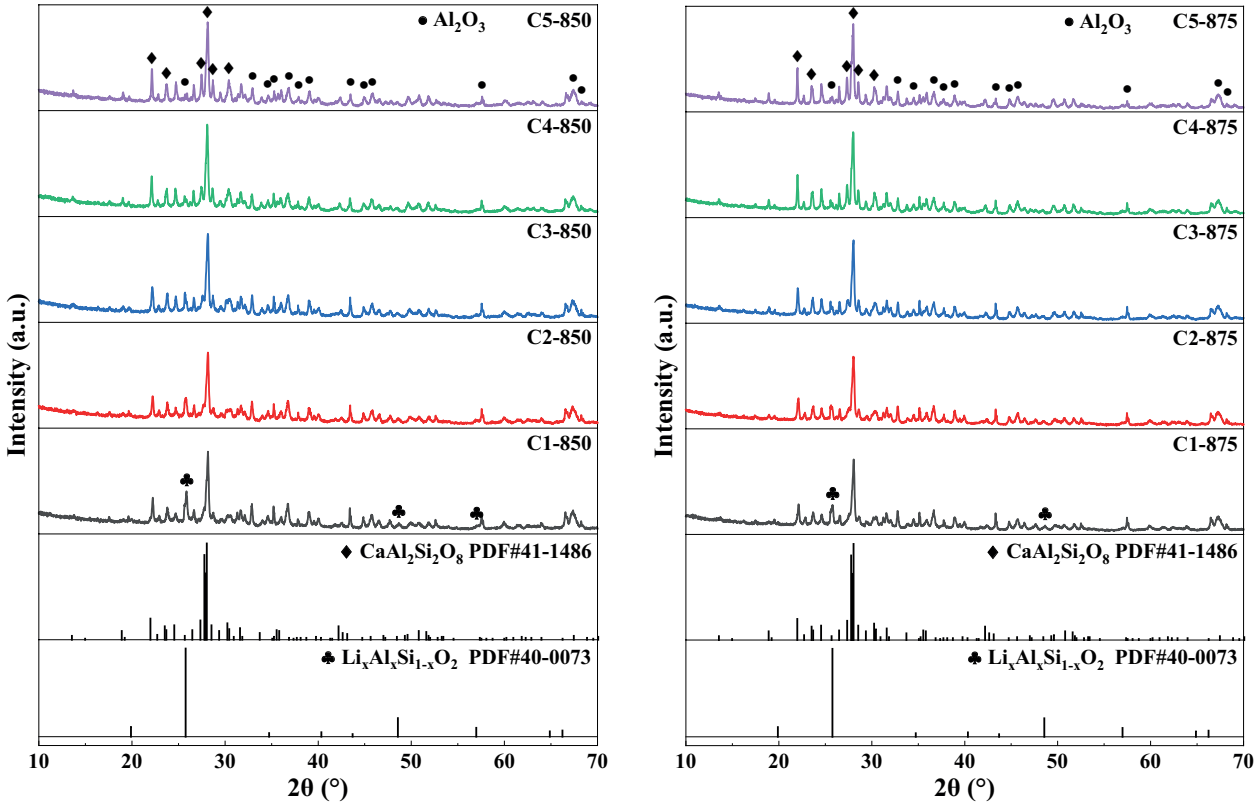

c) 850 °C d) 875 °C

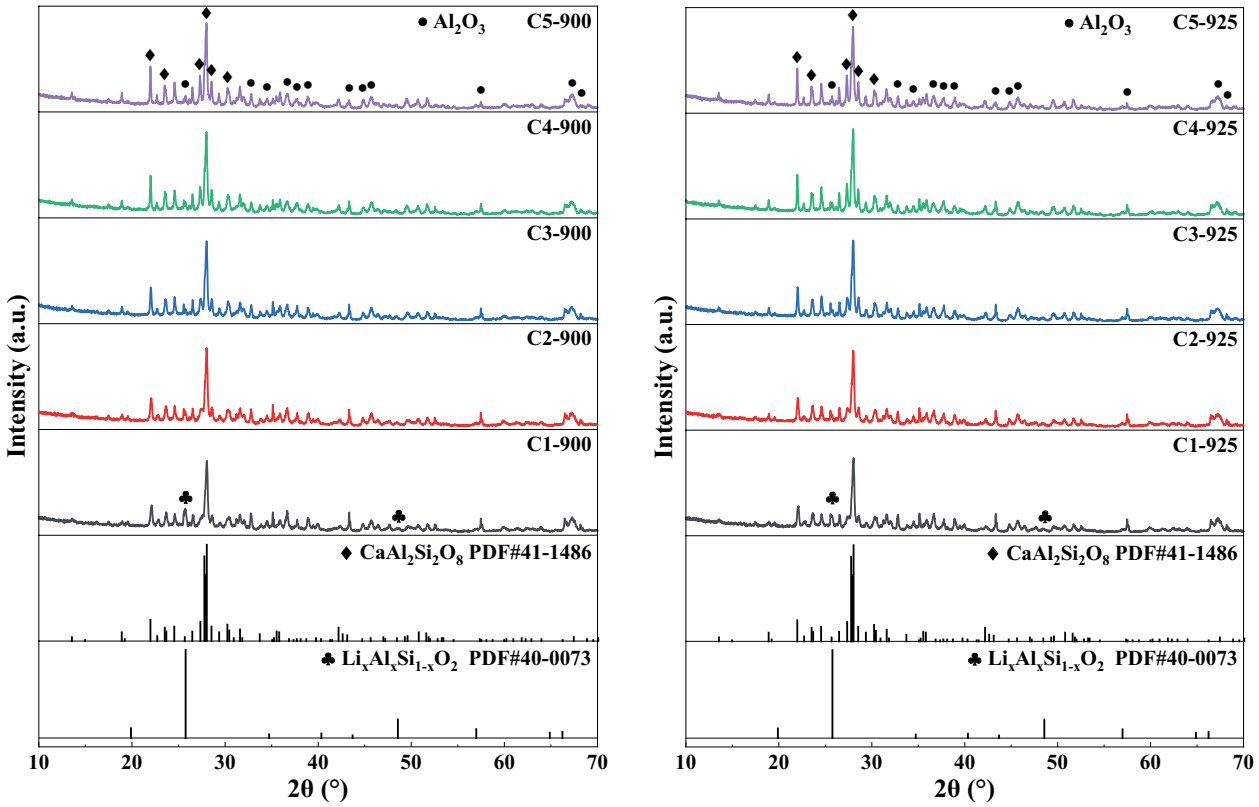

e) 900 °C f) 925 °C

Figure 11. XRD curves of the samples sintered at the different temperatures; b)-e): 825-925 °C.

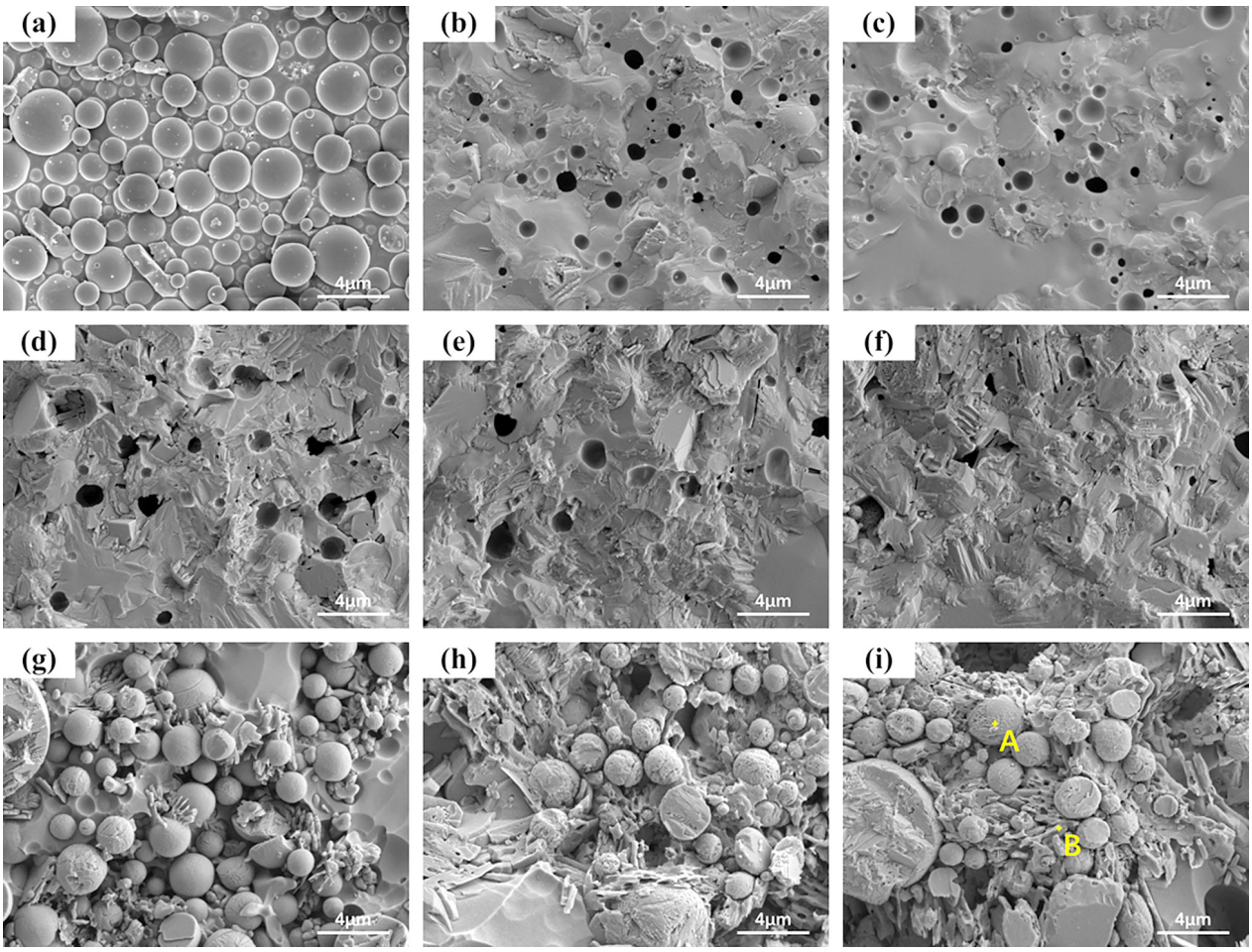

Figure 12. SEM morphology of the micron alumina ball (a); SEM morphology of part of the sample cross-sections; b)-f): C1-825, C3-825, C5-825, C3-875, C5-925; SEM morphology of part of the samples after acid-etching; g)-i): C3-825, C3-875, C3-925.

is shown in Figure 13. The main elements at point A are O and Al, indicating that the spherical object is alumina, and its surface becomes rough, which is caused by the diffusion of alumina in the glass during the sintering process. The main elements at point B are O, Al, Si and Ca, and the ratio of Ca/Si at this point is approximately 0.5. It can be concluded that the columnar structure is anorthite. Due to the diffusion of the alumina, there

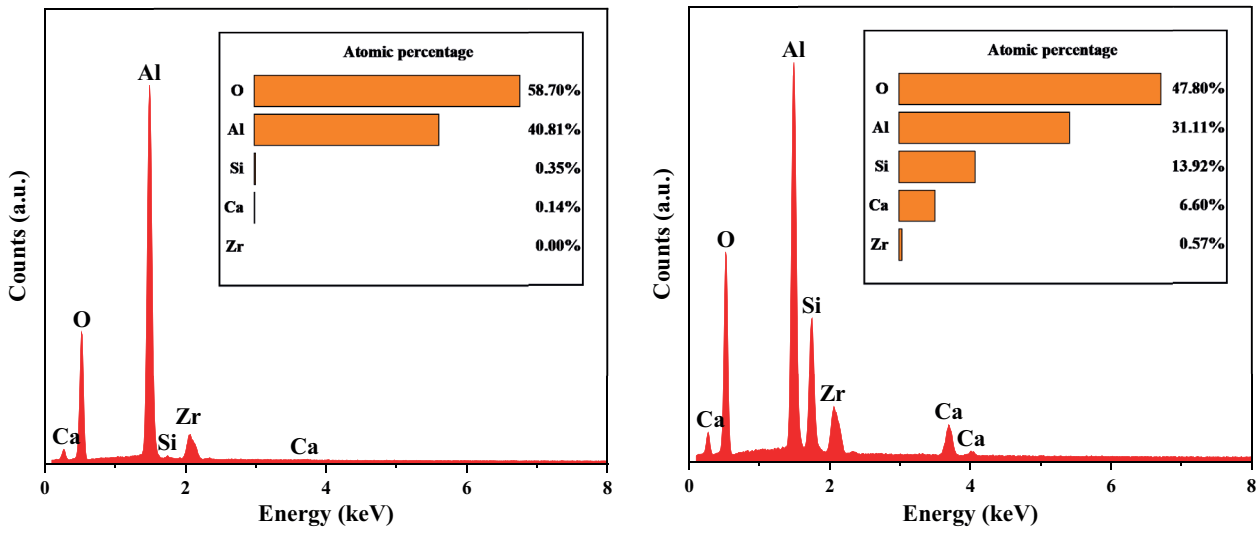

Figure 13. Scanning element composition at points A and B in Figure 12i.

is a large amount of Al and O elements. It can be seen that anorthite is precipitated on the surface of the alumina ball and inside the glass phase. In summary, the sintering of the CBAS glass/Al_2O_3 in this experiment is reactive liquid phase sintering. During the sintering process, Al_2O_3 dissolves in the glass and promotes the precipitation of the anorthite phase, making the glass and Al_2O_3 more closely combined.

Properties of sintered samples

Figure 14 shows the bulk density of the samples sintered at the different temperatures. When the sintering temperature is 825 °C, the bulk density is in the range of 2.90 ~ 2.95 g·cm^{-3}, which is due to the higher density of the alumina. As the content of CaO in the glass increases, the fluidity of the glass liquid at the same temperature increases, which is beneficial to the glass liquid filling the material voids of the material under the capillary force action, so that the bulk density of the sample increases, and reaches the maximum at C4-825. However, C5-825 precipitated a large amount of anorthite, its density is about 2.55 ~ 2.67 g·cm^{-3}, resulting in a gradual decrease in the bulk density. With the increase in the sintering temperature, a large amount of anorthite is precipitated, and the bulk density of the sample is greatly reduced, which is maintained in the range of 2.70 ~ 2.86 g·cm^{-3}. For samples sintered at 850 °C and above, with the increase in the CaO content in the glass, the bulk density first increases and then decreases under the combined effect of the increase in the sintering densification degree and the increase in the anorthite content, and it reaches the maximum value in the C3 or C4 group.

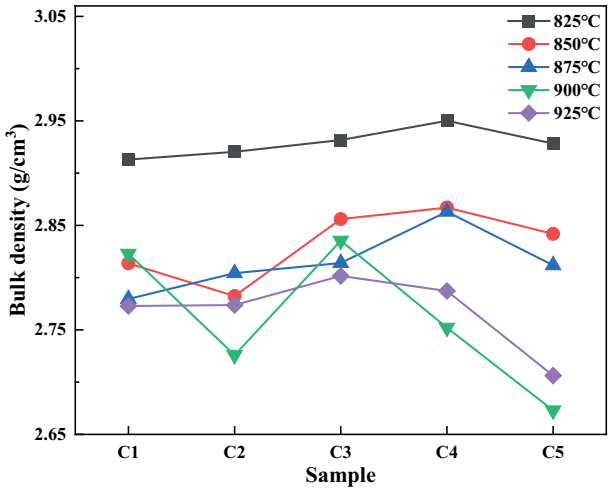

Figure 14. Bulk density of the samples sintered at the different temperatures.

Figure 15 shows the flexural strength of the samples sintered at the different temperatures. When the sintering temperature is 825 °C, the flexural strength of the sample first increases and then decreases with the increase in the CaO content in the glass, and reaches a maximum value of 172.1 MPa at C4-825. With the increase in the CaO content in the glass, on the one hand, the sintering densification gradually increases, and the flexural strength gradually increases. On the other hand, the increase of the non-bridging oxygen in the glass reduces the degree of polymerisation of the glass network, the flexural strength from C4-825 to C5-825 has been reduced. As the sintering temperature increases, there is a maximum value for each group of samples. The flexural strength of the C1 group gradually increases, the flexural strength of the C2-C4 group first increases and then decreases, while the flexural strength of the C5 group gradually decreases. This means that an appropriate amount of anorthite can increase the flexural strength, but once too much anorthite precipitates in the sample, it will reduce the densification of the sample and increase the defects, thus, the flexural strength will decrease accordingly. At the same sintering temperature, the flexural strength first increases and then decreases with the increase in the CaO content in the glass. The maximum flexural strength at each sintering temperature appears in C4-825, C4-850, C4-875, C3-900 and C1- 925, and the flexural strength of C4-850, C3-900 and C1-925 all exceed 190 MPa.

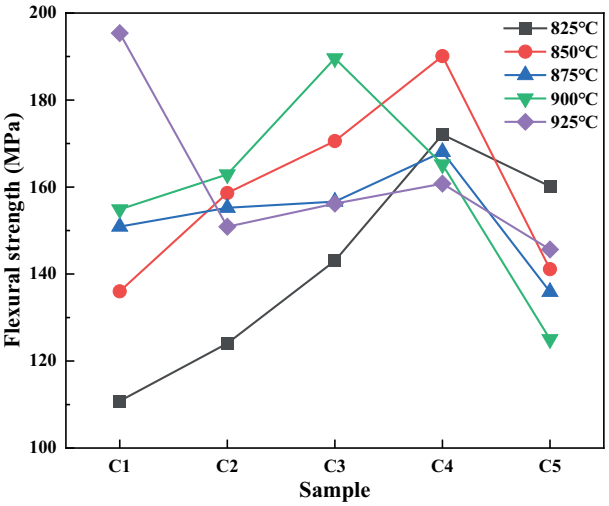

Figure 15. Flexural strength of the samples sintered at the different temperatures.

Figure 16 shows the CTE of the samples sintered at the different temperatures from 30 °C to 500 °C. When the sintering temperature is 825 °C, the CTE of the sample first increases and then decreases with the increase in the CaO content in the glass, and reaches a maximum value of 6.640 × 10^{-6} K^{-1} at C4-825. With the increase in the CaO content in glass, the degree of polymerisation of the glass network decreases, and the crystal phase in the sample changes from the β-quartz solid solution to anorthite, and the CTE increases. With the precipitation of large amount of anorthite, according to the additivity of glass properties, the CTE of samples are close to the CTE of anorthite, due to the CTE of

anorthite being 4.5 × 10^{-6} K^{-1} (20 - 500 °C) [40], the CTE begins to decrease after C4-825 reaches its maximum value. Due to the precipitation of a large amount of the anorthite phase in the samples sintered at 850 °C and higher, the CTE of each group from 825 °C to 850 °C has been greatly reduced. Except for C5-850, the CTE of the samples sintered at 850 °C are all near 6.0 × 10^{-6} K^{-1}. With the increase in the sintering temperature, the CTE shows a trend of first decreasing and then increasing, and there is a minimum value at 875 °C. This is because the increase in the sintering temperature is conducive to sintering compaction, where the sintering densification decreases, and CTE exists certain degree of increase. In summary, the CTE of the samples sintered at the different temperatures is in the range of 5.711 × 10^{-6} ~ 6.640 × 10^{-6} K^{-1}, which matches the thermal expansion coefficient of common semiconductor materials.

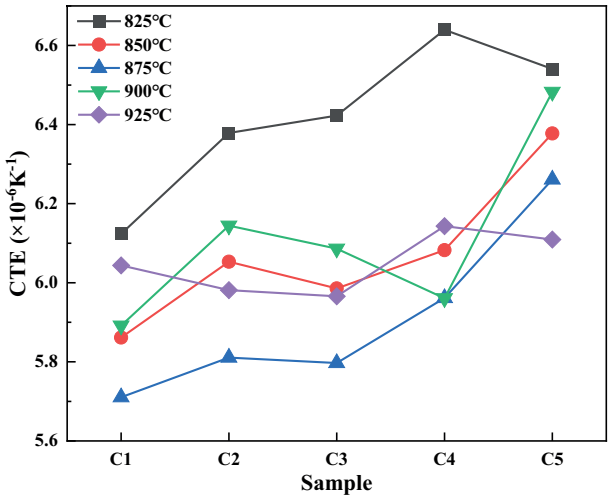

Figure 16. CTE of the samples sintered at the different temperatures (30-500 °C).

CONCLUSIONS

This paper studied the influence of the CaO content in the glass on the $CaO–B_2O_3–Al_2O_3–SiO_2$ glass/Al_2O_3 system LTCC materials. The main conclusions are listed as follows:

- With an increase in the CaO content in the CBAS glass, the polymerisation degree of the glass network decreases, thereby reducing the glass transition temperature, softening temperature and crystallisation temperature of the parent glass and the sintering densification temperature of the CBAS glass/Al_2O_3, the sintering activation energy first decreases and then increases.
- In addition to alumina, the crystalline phases of the sintered samples include β-quartz solid solution and anorthite. With an increase in the CaO content in the glass and the sintering temperature, the anorthite gradually increases, the alumina and β-quartz solid solution gradually decreases. During the sintering process, part of alumina dissolves into the glass liquid to promote the precipitation of anorthite. The anorthite phase precipitates on the surface of glass phase and the alumina ball in the sample.
- The precipitation of anorthite reduces the bulk density of the samples. An appropriate amount of anorthite can improve the flexural strength of the samples, and the best flexural strength of some samples exceeds 190 MPa in the experiment. The CTE of the sintered samples is in the range of 5.711~6.640×10^{-6} K^{-1}, which matches the thermal expansion coefficient of common semiconductor materials.

Acknowledgement

This work was supported by the State Key Laboratory of Advanced Materials and Electronic Components (grant number FH2018sk201). The authors express their sincere gratitude to the 'Material Research and Testing Center of Wuhan University of Technology'.

REFERENCES

1. Ullah U., Mahyuddin N., Arifin Z., Abdullah M.Z., Marzuki A. (2015): Antenna in LTCC technologies: a review and the current state of the art. *IEEE Antennas and Propagation Magazine, 57*(2), 241-260. doi: 10.1109/MAP.2015.2414668
2. Sebastian M. T., Jantunen H. (2013): Low loss dielectric materials for LTCC applications: a review. *International Materials Reviews, 53*(2), 57-90. doi: 10.1179/174328008X277524
3. Baker A., Lanagan M., Randall C., Semouchkina E., Semouchkin G., Rajab Z. K., Eitel R. (2005): Integration concepts for the fabrication of LTCC structures. *International Journal of Applied Ceramic Technology, 2*(6): 514-520. doi: 10.1111/j.1744-7402.2005.02052.x
4. Ren H., Hao L, Peng H, Dang M., Xie T., Zhang Y., Jiang S., Yao X., Lin H., Luo L. (2018): Investigation on low-temperature sinterable behavior and tunable dielectric properties of BLMT glass-$Li_2ZnTi_3O_8$ composite ceramics. *Journal of the European Ceramic Society, 38*(10), 3498-3504. doi: 10.1016/j.jeurceramsoc.2018.03.053
5. Li B., Duan D., Long Q. (2016): Effects of TiO_2 on microstructures and properties of $Li_2O–Al_2O_3–SiO_2$ glass-ceramics for LTCC substrates. *Journal of Materials Science: Materials in Electronics, 27*(7), 7240-7245. doi: 10.1007/s10854-016-4690-3
6. Yang F., Yuan Y., Li J., Zhang C., Tong J., Meng F. (2020): Sintering behavior and properties of CABS/$MgAl_2O_4$ composite for LTCC applications. *Journal of Materials Science: Materials in Electronics, 31*(20), 17375-17380. doi: 10.1007/s10854-020-04293-8
7. Sebastian M. T., Ubic R., Jantunen H. (2015): Low-loss dielectric ceramic materials and their properties. *International Materials Reviews, 60*(7), 392-412. doi: 10.1179/1743280415Y.0000000007

8. Qin T., Zhong C., Yang H., Qin Y., Zhang S. (2019): Investigation on glass-forming ability, flexural strength and microwave dielectric properties of Al_2O_3-doped LMZBS glasses. *Ceramics International, 45*(8), 10899-10906. doi: 10.1016/j.ceramint.2019.02.168
9. Montedo O. R. K., Hotza D., De Oliveira A. P. N., Meszaros R., Travitzky N., Greil Peter. (2012): Crystallisation Kinetics of a β-Spodumene-Based Glass Ceramic. *Advances in Materials Science and Engineering, 2012*, 1-8. doi: 10.1155/2012/52
10. Li B., Duan D., Long Q. (2015): Influences of ZrO_2 on microstructures and properties of Li_2O–Al_2O_3–SiO_2 glass-ceramics for LTCC applications. *Journal of Materials Science: Materials in Electronics, 27*(1), 134-139. doi: 10.1007/s10854-015-3728-2
11. Qing Z. J., Li B., Duan D. A., Li H., Li Y. X., Zhang S. R. (2016): Phase evolution and properties of Li_2O–Al_2O_3––SiO_2-based glass-ceramic for LTCC applications. *Key Engineering Materials, 697*, 257-261. doi: 10.4028/www.scientific.net/KEM.697.257
12. Qin Y., Zhong C., Yang H., Qin T., Yuan Y., Tang B., Zhang S. (2019): Enhanced thermal and mechanical properties of Li-Al-Si composites with K_2O–B_2O_3–SiO_2 glass for LTCC application. *Ceramics International, 45*(12), 15654-15659. doi: 10.1016/j.ceramint.2019.05.077
13. Gu S. I., Shin H. S., Yeo D. H., Nahn S. (2013): Crystal phase evolution, sintering, and strength of anorthite-based LTCC materials by substitution of M^{2+} (M = Mg, Sr, Ba) for Ca^{2+}. *Metals and Materials International, 19*(3), 399-404. doi: 10.1007/s12540-013-3004-z
14. Wu C. W., Jean J. H., Pinckney L. (2016): Crystallization kinetics and dielectric properties of a low-fire CaO–Al_2O_3––SiO_2 glass + alumina system. *Journal of the American Ceramic Society, 99*(8), 2664-2671. doi: 10.1111/jace.14271
15. Sun Z., Li W., Liu Y., Zhang H., Zhu D., Sun H., Hu C., Chen S. (2019) Design and preparation of a novel degradable low-temperature co-fired ceramic (LTCC) composites. *Ceramics International, 45*(6), 7001-7010. doi: 10.1016/j.ceramint.2018.12.201
16. Yang F., Tan Y., Yuan Y., Li J., Zhang C., Liu Y., Tong J., Meng F. (2020): Sintering behavior and properties of Li_2O––MgO–ZnO–B_2O_3–SiO_2 ceramic composites for applications in low temperature co-fired ceramic (LTCC) technologies. *Journal of Materials Science: Materials in Electronics, 32*(1), 125-132. doi: 10.1007/s10854-020-04718-4
17. Wang F., Chen X., Zhang W., Mao H. (2018): Synthesis and characterization of borosilicate glass/β-spodumene/Al_2O_3 composites with low CTE value for LTCC applications. *Journal of Materials Science: Materials in Electronics, 29*(11), 9038-9044. doi: 10.1007/s10854-018-8929-z
18. Qin T., Zhong C., Tang B., Zhan S. (2021): A novel type of composite LTCC material for high flexural strength application. *Journal of the European Ceramic Society, 41*(2), 1342-1351. doi: 10.1016/j.jeurceramsoc.2020.09.046
19. Sawhill H. T. (1988): Materials compatibility and co-sintering aspects in low temperature co-fired ceramic packages. *Cofire Technology: Ceramic Engineering and Science Proceedings, 9*, 1603-1617. doi: 10.1002/9780470310519.ch5
20. Dai S. (2012): Densification and crystallization in crystallizable low temperature co-fired ceramics. *Journal of Materials Science, 47*(11), 4579-4584. doi: 10.1007/s10853-012-6318-1
21. Luo X., Tao H., Li P., Fu Y., Zhou H. (2020): Properties of borosilicate glass/Al_2O_3 composites with different Al_2O_3 concentrations for LTCC applications. *Journal of Materials Science: Materials in Electronics, 31*(17), 14069-14077. doi: 10.1007/s10854-020-03961-z
22. Wang F., Lou Y. H., Li Z. J., Lei W., Lu Y., Dong Z. W., Lu W. Z. (2021): Improved flexural strength and dielectric loss in Al_2O_3-based LTCC with La_2O_3–CaO–B_2O_3–SiO_2 glass. *Ceramics International, 47*(7), 9955-9960. doi: 10.1016/j.ceramint.2020.12.140
23. Yan T., Zhang W., Mao H., Mao H., Chen X., Bai S. (2019): The effect of CaO/SiO_2 and B_2O_3 on the sintering contraction behaviors of CaO–B_2O_3–SiO_2 glass-ceramics. *International Journal of Modern Physics B, 33*(09), 1950070. doi: 10.1142/s021797921950070x
24. Shang Y., Zhong C., Jia R., Xiong H., Li H., Li X., Jian X. (2019): Preparation of low-permittivity K_2O–B_2O_3–SiO_2––Al_2O_3 composites without the addition of glass. *Nanotechnology Reviews, 8*(1), 459-466. doi: 10.1515/ntrev-2019-0041
25. Chen G. H., Tang L. J., Cheng J., Jiang M. H. (2009): Synthesis and characterization of CBS glass/ceramic composites for LTCC application. *Journal of Alloys and Compounds, 478*(1-2), 858-862. doi: 10.1016/j.jallcom.2008.11.163
26. Ko M., Lyoo S. (2011): Novel double-layer structure LTCC substrate with enhanced flexural and adhesions strengths. *International Journal of Applied Ceramic Technology, 8*(1), 180-186. doi: 10.1111/j.1744-7402.2009.02425.x
27. Shi J., He F., Ye C., Hu L., Xie J., Yang H., Liu X. (2017): Preparation and characterization of CaO–Al_2O_3–SiO_2 glass-ceramics from molybdenum tailings. *Materials Chemistry and Physics, 197*, 57-64. doi: 10.1016/j.matchemphys.2017.05.028
28. Doweidar H., El-Damrawi G., Al-Zaibani M. (2013): Distribution of species in Na_2O–CaO–B_2O_3 glasses as probed by FTIR. *Vibrational Spectroscopy, 68*, 91-95. doi: 10.1016/j.vibspec.2013.05.015
29. Shi J., He F., Xie J., Liu X., Yang H. (2019): Effect of heat treatments on the Li_2O–Al_2O_3–SiO_2–B_2O_3–BaO glass-ceramic bond and the glass-ceramic bond cBN grinding tools. *International Journal of Refractory Metals and Hard Materials, 78*, 201-209. doi: 10.1016/j.ijrmhm.2018.09.015
30. Deng L., Jia R., Yun F., Zhang X., Li H., Zhang M., Jia X., Ren D., Li B. (2020): Influence of Cr_2O_3 on the viscosity and crystallization behavior of glass ceramics based on blast furnace slag. *Materials Chemistry and Physics, 240*, 122212. doi: 10.1016/j.matchemphys.2019.122212
31. Chen M., He F., Shi J., Xie J., Yang H., Wan P. (2019): Low Li_2O content study in Li_2O–Al_2O_3–SiO_2 glass-ceramics. *Journal of the European Ceramic Society, 39*(15), 4988-4995. doi: 10.1016/j.jeurceramsoc.2019.07.032
32. Banjuraizah J., Mohamad H., Ahmad Z. A. (2011): Effect of impurities content from minerals on phase transformation, densification and crystallization of α-cordierite glass-ceramic. *Journal of Alloys and Compounds, 509*(28), 7645-7651. doi: 10.1016/j.jallcom.2011.04.129
33. Shi J., He F., Xie J., Liu X., Yang H. (2018): Effects of Na_2O/BaO ratio on the structure and the physical properties of low-temperature glass-ceramic vitrified bonds. *Ceramics International, 44*(9), 10871-10877. doi: 10.1016/j.ceramint.2018.03.140

34. Zhang B., He F., Cao X., Wei M., Zheng C., Xie J. (2022): The effect of TiO_2 and B_2O_3 on sintering behavior and crystallization behavior of SrO–BaO–B_2O_3–SiO_2 glass-ceramics. *Ceramics International, 48*(5), 7013-7023. doi: 10.1016/j.ceramint.2021.11.259
35. Aksay I. A., Hoge C. E., Pask J. A. (1974): Wetting under chemical equilibrium and nonequilibrium conditions. *The Journal of Physical Chemistry, 78*(12), 1178-1183. doi: 10.1021/j100605a009
36. Mohanram A., Messing G. L., Green D. J. (2005): Densification and sintering viscosity of low-temperature co-fired ceramics. *Journal of the American Ceramic Society, 88*(10), 2681-2689. doi: 10.1111/j.1551-2916.2005.00497.x
37. Li B., Bian H. B., Jing K. (2019): Influence of Sm_2O_3 additive on BaO–Al_2O_3–B_2O_3–SiO_2 glass-ceramics for CBGA package. *Key Engineering Materials, 803*, 88-92. doi: 10.4028/www.scientific.net/KEM.803.88
38. Qin T., Zhong C., Qin Y., Tang B., Zhang S. (2019): Low-temperature sintering mechanism and microwave dielectric properties of $ZnAl_2O_4$–LMZBS composites. *Journal of Alloys and Compounds, 797*, 744-753. doi: 10.1016/j.jallcom.2019.05.141
39. Cui X. M., He Y., Liang Z. Y., Zhang H., Zhou J. (2010): Different microstructure BaO–B_2O_3–SiO_2 glass/ceramic composites depending on high-temperature wetting affinity. *Ceramics International, 36*(4), 1473-1478.doi: 10.1016/j.ceramint.2010.01.005
40. Barbieri L., Bondioli F., Lancellotti I., Leonelli C. Montorsi M. Ferrari A. M., Miselli P. (2005): The Anorthite-Diopside System: Structural and Devitrification Study. Part II: Crystallinity Analysis by the Rietveld-RIR Method. *Journal of the American Ceramic Society, 88*(11), 3131-3136. doi: 10.1111/j.1551-2916.2005.00578.x